Solid Freeform Fabrication 2022: Proceedings of the 33rd Annual International Solid Freeform Fabrication Symposium – An Additive Manufacturing Conference
Reviewed Paper

STUDY OF PROXIMITY EFFECT IN PROJECTION-BASED MICRO STEREOLITHOGRAPHY PROCESS

Aditya Chivate[1], Zipeng Guo[1], Chi Zhou[1]*

[1]Department of Industrial and Systems Engineering, University at Buffalo, The State University of New York, Buffalo, NY 14260

Abstract

Micro Projection-based stereolithography (μPSL) is a powerful technique that has the potential to disrupt microfabrication. However, a significant challenge that plagues μPSL is the local change in thresholds depending on the pitch between adjacent features, and having features in close spatial proximity generates undesired artifacts. This is termed as "proximity effect," which strongly limits the attainable fabrication resolution. This can be linked to pixel-pixel light interactions and is found to affect the process in spatial as well as temporal domains. Despite tormenting researchers for a long, not much has been done to study these effects in DLP printing. Models developed for laser-based systems can be used to explain the proximity effect in μPSL. However, they still rely on hindsight observations, fail to consider the effects of large area projection, and fail to explain how the local change in thresholds affects the part size. This research uses in-situ observation systems to study the spatial and temporal proximity effects in single-shot PSL microfabrication. We briefly illustrate the role of oxygen in the proximity effect and lay the foundations to better understand the proximity effect in periodic structures with micronic inter-feature distances.

Keywords: Proximity effects, oxygen inhibition, cross-talk, stereolithography

Introduction

Additive manufacturing is changing how we fabricate things and has attracted attention in several applications ranging from biomedical devices to automotive components. With advancements in technology, AM processes can now be used to fabricate micron-scaled features and biologically inspired textured surfaces with patterned structures finding applications in photonics, micromechanics, microbiology, targeted drug delivery, and optics [1-6]. Two-Photon Polymerization (2PP) is at the forefront of this manufacturing and has long been used for fabricating sub-micron features. Efforts are now being made to search for alternatives as 2PP has print speeds of 10μm/s making it incredibly slow [7]. Despite the efforts made in mass parallelization, the high costs associated with the tools make their entry into the industrial setting challenging[8, 9]. Digital Light Projection (DLP) based stereolithography is the most versatile technology for rapid prototyping and has seen a considerable push in its benchmarks in recent years. It has the potential to overtake 2PP due to its high throughput and economic setup costs [10]. DLP uses a series of mask images to fabricate complex, high-resolution 3D features. As a complete digital mask is projected during each instance, the build size is dependent on the

projection size, which is easy to manipulate by adjusting the optical setup to the desired magnification. The desired characteristic of micron-scaled fabrication is the feature resolution and density [1]. Feature resolution refers to the size of the smallest feature that can be printed, and feature density refers to the number of high-resolution features packed in a specified area. The feature resolution depends on the pixel size and can be arbitrarily reduced by changing the optics and light engines, but reducing feature separation remains challenging. While this can be achieved by packing the patterns closely in the digital mask, the closeness of these features tends to influence each other, causing undesired effects like over-curing, sporadic connections, feature bending, and non-uniformity. This loss in the feature resolution due to the propinquity is termed "proximity-effect" [11, 12]. A number of potential reasons could contribute to the proximity effect, including the polymer properties, light scattering and spreading, thermal or molecular diffusion, and dose addition due to subsequent projections [13]. However, there is neither a precise knowledge about the underlying mechanisms of the proximity effect, nor is the effect well characterized in strength or spatial-temporal domain typical to DLP printing.

In DLP technology, local polymerization should take place only in the irradiation region. In practice, the light bleeds into neighboring pixels, causing an envelope of semi-cured resin around the actual feature [14]. Light damage occurs when the amount of energy absorbed by the photopolymer exceeds the required threshold. Two primary reasons may cause this over-exposure; either the time difference between two subsequent exposures is too small for the oxygen to replenish, or the gap between the adjacent features is smaller than the light bleeding threshold. If the cross-talking between the features occurs due to the closeness of the features, it is termed as "spatial proximity effect"; if it occurs because of the time delay between subsequent projections, it is termed as "temporal proximity effect." These effects are present across scales but are detrimental, especially in micron-scaled patterned structures.

In this research, we quantitatively characterize the strength of the proximity effect on spatial and temporal scales specific to DLP printing. We use a DMD light modulator to precisely control the mask shapes and inter-feature spacing. The impact of spatial distribution on the photopolymerization process is studied, and a general decay function is derived based on the collected data. Multi-mask projection strategies to circumvent the spatial proximity effect are presented, and the temporal effect arising due to the time delay between the exposures is studied. We hypothesize that oxygen plays a vital role in determining the extent of the proximity effect. We present experimental evidence of the effect of oxygen. These results provide new insights into the spatial and temporal effects in DLP printing and indicate that oxygen strongly influences the feature size on a comparable length and time scale.

Experimental Setup

The experimental setup consisted of two main components, a projection-based photocuring setup and an observation system consisting of a confocal microscope-based observation system for spatial observations from the top and a schlieren-based observation system for side-ways observation.

Digital Light Projection setup

This research uses a OmniCure S1500 UV mercury lamp system combined with a 405 nm UV filter for illumination. The light is delivered via a 0.37 NA light guide with a 3mm output diameter, and all the experiments were performed at 40% light output, giving an irradiance of 208μW/cm^2. Light coming from the lamp is collimated using a $f = 200$mm achromatic doublet lens and was shone on a high-performance light engine from Vialux used for digital mask generation. The DMD has a resolution of 1920 × 1080 with an individual micromirror measuring 10.8 μm on each side and a pitch of 1 μm. The light reflecting from the DMD was passed through a set of focusing lenses on forming a focused image on the vat surface. The setup was compacted by using a flat mirror to deviate the light's path while providing the same optical distance. This setup allows tunability by changing the optics. Adjustable optics enable adaptable magnification for tuning the projected image. The optical system was adjusted to achieve a 1:5 magnification by using a 5x objective lens and later to achieve 1.5:1 magnification to test the system's robustness and study the proximity effect at varying scales. A bi-telecentric system was used for projection in both cases. A telecentric system ensures constant magnification regardless of the distance or location in the field of view. As the study's objective was to study the proximity effect in the spatial and temporal domain, a stationary platform submerged in the vat was used. Binary masks were projected from the bottom of the vat made from an all-side transparent UV-transparent cuvette. A high-speed CMOS camera from AmScope was used to capture the voxel growth process from the side, whereas a CCD camera from EIA Japan captured the spatial images from the top. A white LED with a light guide illuminated the schlieren setup.

Observation setup

The observation setup consisted of two components, a schlieren-based system to observe the voxel growth from the side and a confocal system for spatial observations from the top. Schlieren exploits the changes in optical density of the resin as the polymerization progresses to give a detailed image of the voxel that is not easily visible to the naked eyes. A lens-based schlieren was used with a magnification system to observe the voxels from the side. The second component of the observation system consists of a confocal setup with a high magnification objective lens and a UV camera. The typical system has a UV camera and an objective lens placed at the focus of a $f = 150$ mm achromatic doublet lens on either side. As the photopolymerization progresses, there is a local change in the optical density. This change causes the projected light to spread in the X-Y plane beyond the mask dimensions. A high-speed camera can capture this process frame by frame, and depending on the spread; the proximity effects can be quantified. We use a 405nm UV filter, and the resin used for these experiments absorbs most of the UV light. A regular camera cannot detect the light transmitted through the resin, so a UV camera was used.

The schlieren technique was developed in the early 1800s which exploits the bending of light due to refractive index change corresponding to alterations in the optical density gradients in transparent media to generate images with contrast [15]. It is widely used to characterize fluid flows. A lens-based schlieren system as developed for this research has three main components:

illumination source, lenses and knife-edge. The system uses collimated white light for illuminating the test area which is placed between the collimating lens and a pair of focusing lens. A knife-edge is placed at the focal point of the focusing lenses such that it cuts half the light passing through. When there is a change in the refractive index of the fluid in the test area corresponding to the resin polymerization, collimated light passing through it bends following Snell's law. When there is a change in the refractive index gradient, there is a corresponding shift in the light spot at the focus. This allows a local change in the number of rays that are blocked by the knife edge giving rise to a region of contrast depending on the bending direction and an image is generated on a virtual screen [16-18]. A camera with a confocal magnification setup is attached to the system as the parts under consideration are sub-50μm.

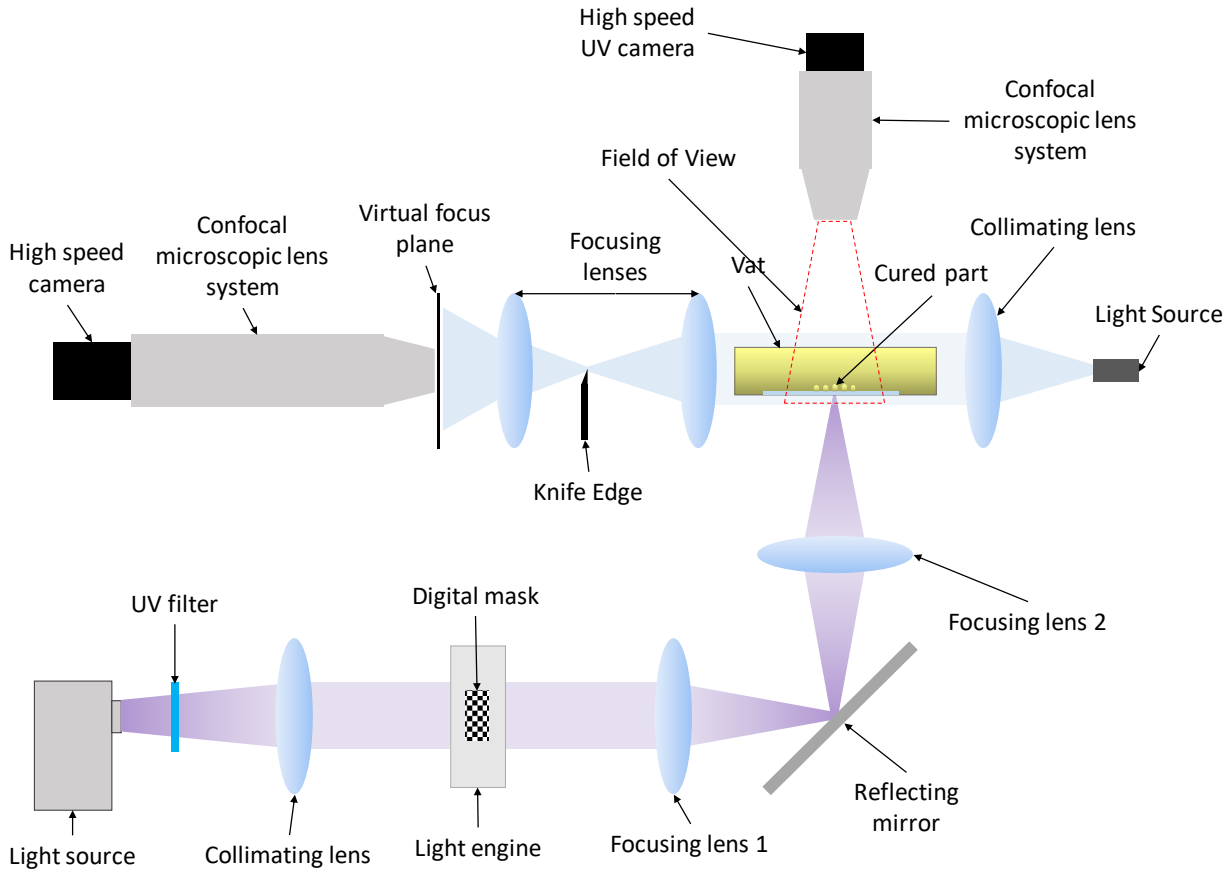

Figure 1 Schematic of projection and observation system

Materials and Methods

The acrylate-based resin was commercially procured from AnyCubic, and 2,4-Di-tert-butyl-6-(5-chloro-2H-benzo-triazol-2-yl)phenol (Tinuvin 327) (procured from Sigma Aldrich) was used as a UV dye. 1% w/w dye was mixed with the resin by dissolving it in chloroform and stirring it at 500 rpm for 15 minutes. The printed samples were cleaned using 90% IPA followed by a bath of DI water inside a sonicator. To study the proximity effect in the spatial domain, binary

masks with periodic patterns having different pitches were projected at a constant light intensity of 208μW/cm^2. Temporal effects were studied by projecting two separate non-overlapping digital masks with a varying time delay between subsequent projections. The effect of oxygen was studied by preparing two additional samples. The oxygen-rich sample was prepared by bubbling supplemental oxygen into the resin for 60 seconds in a vacuum container to make sure supplemental oxygen was diffused into the resin. Another sample was deprived of oxygen by vacuuming out all the air and purging in carbon dioxide to displace oxygen. Additional carbon dioxide was poured into the vat and was sealed to avoid interactions with the atmospheric air.

Results and Discussions

This section presents the experimental validation using the free-form voxel growth experiment. Particularly, the spatial spreading, cross-talking, temporal effects, and role of oxygen are measured and characterized using SEM.

Spatial Effect

Feature density is the desired characteristic in the microfabrication of periodically patterned structures like microlens arrays or microneedles. Higher packing density has its advantages due to its unique optical and structural properties. Efforts are being made to fabricate high-resolution features as close as possible, but this comes at a cost. The spatial closeness of the features gives rise to cross-talking between the features. This effect is more prevalent in the proximity of the actual illuminated spot. It can be attributed to the light spreading into neighboring pixels, creating a halo around the actual projection, also known as the sphere of influence. The effect of cross-talk starts fading out when the spatial distance between the features increases.

Observations from the confocal microscopic system reveal this spatial effect in-situ. It is seen that the neighboring features influence the part growth, and for the same exposure, the features that are in close proximity tend to grow bigger. **Figure *2*** (a) and (c) show the projected image, and **Figure *2*** (b) and (d) shows the observed image after 8 seconds of exposure. The halo around the features in **Figure *2*** (b) and (d) can be attributed to the scattering of light as the refractive index changes upon polymerization.

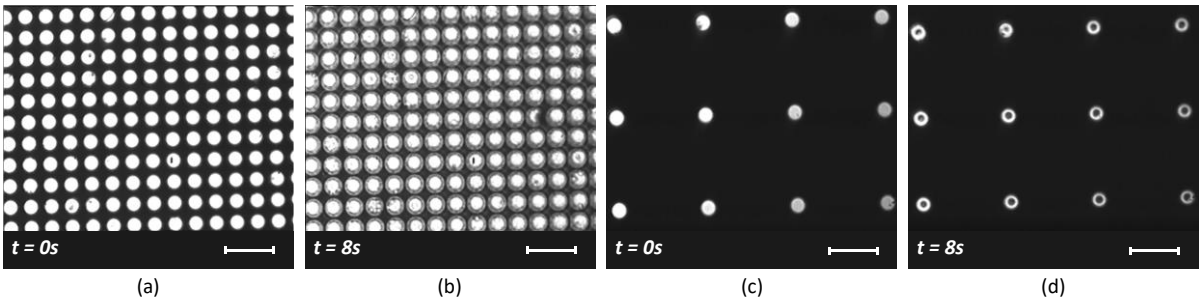

Figure 2 Spatial proximity effect as observed from the designed system for a feature size of 20 μm (a) pitch = 20 μm (b) polymerized part (c) pitch = 200 μm (d) polymerized part. Scale bar = 50 μm

The cross-talking effect is more prevalent within a specific region and fades out as the spatial distance between the features increases. As shown in **Figure *3*** (a), the spatial proximity effect decays exponentially and is not significant beyond 80µm gap as the size deviation is well within the acceptable limits for the desired microlens applications. This is specific to this resin, but the overall trend is also similar for other materials. **Figure *3*** (b) shows sporadic connections between the features that arise due to the cross-talking between the neighboring features, and the effect seems to lessen as the gap between them increases. **Figure *3*** (d) is the control that has features as desired. Whereas **Figure *3*** (e) depicts the features that are smaller than desired for the same amount of exposure as they are sparsely spread, thus preventing any significant cross-talking from influencing the size.

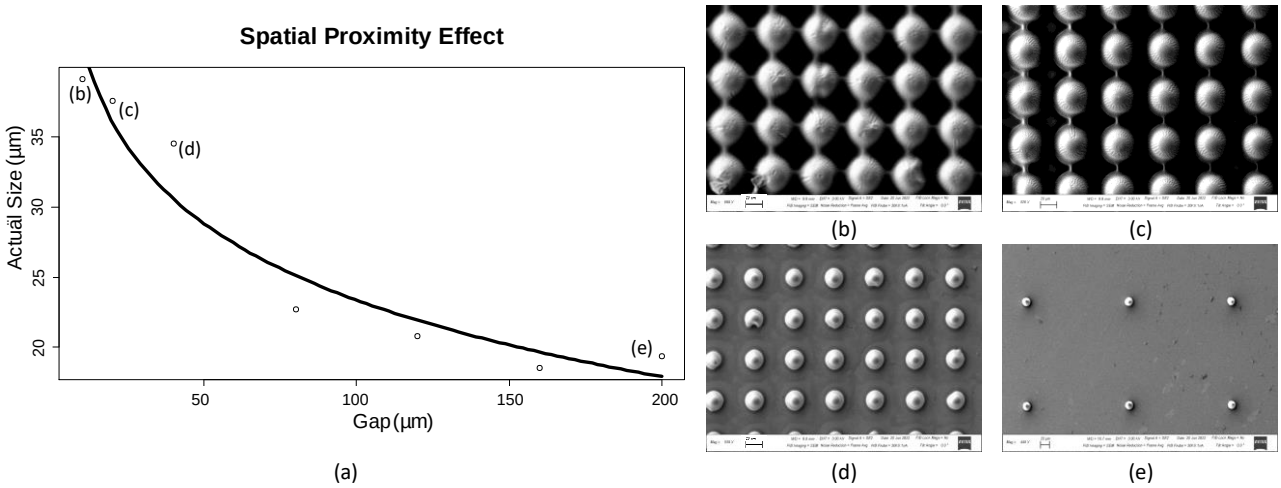

Figure 3 (a) Graph showing how spatial effect decays as the inter-feature gap increases, features with different pitch as observed under SEM (b) pitch = 10 µm (c) pitch = 20 µm (d) pitch = 40 µm (e) pitch = 200 µm (SEM scale bar = 20 µm)

The spatial cross-talking effect is evident only within a specific sphere of influence. It depends on the light intensity, light spreading, and the number of features present on either side. **Figure *4*** (a) shows a schematic of the additive effect of light bleeding into neighboring pixels. The features in the center are influenced by the light from its eight immediate neighbors. The features on the sides are influenced by five neighbors, whereas the features on the corners get contributions only from three of its neighbors. This non-uniformity in the exposure is more prevalent within the sphere of influence and is dependent on the chemical composition of the resin, wavelength of light, and the depth of focus [13]. When the gap between the individual features is more than a certain value, the additive effect of light intensity is not very predominant. The distance beyond which the additive effect weakens is generally determined by the chemical properties of the resin. Based on the UV resin used in these experiments, the effect is more prevalent when the gap between adjacent features is relatively small. **Figure *4*** (b) shows the non-uniformity in the size of the printed microlens at the corner. This can be attributed to the fact that for all the other lenses, the size is due to the additive effect of light from all the neighbors. Whereas for the microlens at the corner, the neighboring features exist only on one side.

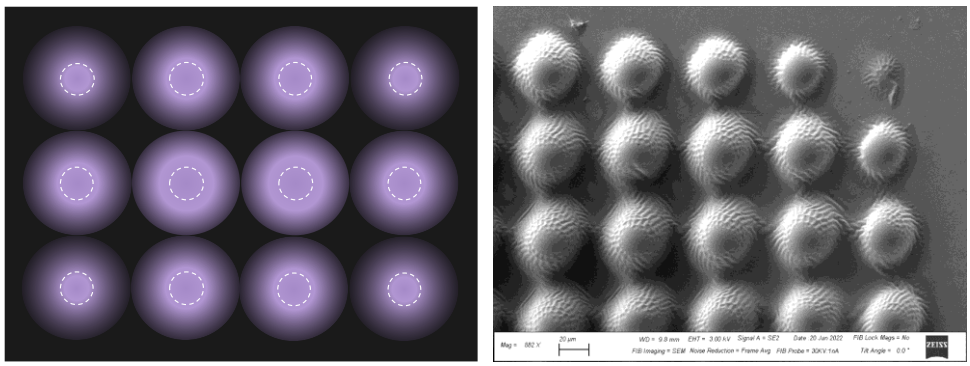

Figure 4 (a) Schematic of light bleeding into neighboring pixels in the spatial domain (b) SEM image depicting spatial proximity effect at corners (SEM scale bar = 20 µm)

Temporal effect

As discussed in the previous section, the spatial proximity effect has made the adoption of µPSL challenging and efforts need to be made to find alternatives to overcome this effect. Using sequential masks with alternating patterns is a possible way to circumvent the spatial proximity effect. In this method, multiple masks with larger spatial gaps and alternating feature locations are projected sequentially. **Figure *5*** (b) and (c) show the masks for the first and second projections. The masks have patterns at alternating locations. The dotted lines in **Figure *5*** (c) are representative of the cured features and are not a part of the actual mask. Ideally, we should take advantage of breaking the sphere of influence and prevent the effect of light bleeding. Despite this being a great alternative, in practice, the time delay between two projections plays a critical role in determining the feature resolution. Experiments have shown that if the delay between subsequent projections is small, the second projection tends to absorb more energy resulting in thicker features. This is termed the proximity effect in the temporal domain or simply the temporal effect.

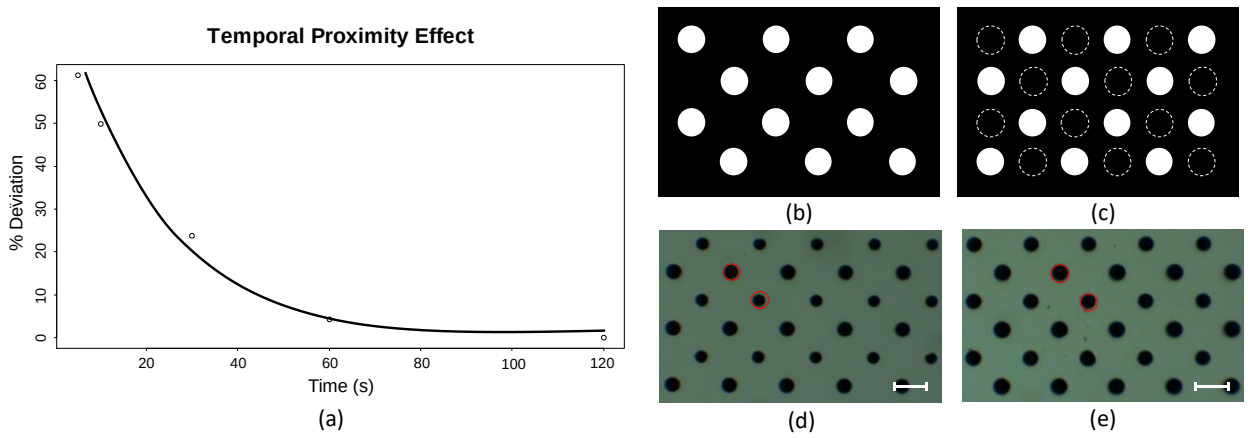

Figure 5 (a) Graph showing how the temporal effect fades out with time, (b) mask for first exposure, (c) mask for second exposure, temporal effect as seen under a microscope when (d) time delay is 10s, and (e) time delay is 60s (red circle represents actual part) (scale bar = 50µm)

The temporal proximity effect fades out as the time delay increases and behaves like a closely packed single projection. **Figure *5*** (a) shows the exponential decay of the temporal effect as the time delay between projections increases. The graph represents the percent deviation in size between the features printed from the first and second projections. As seen from **Figure *5*** (b), when the time difference is small, the features printed due to the second projection tend to be relatively larger. It can be seen from **Figure *5*** (c) and (e) that with increased delay, the features are visually indistinguishable, and there is an increase in the uniformity of the features. It is also evident that planning the images with alternating patterns helps overcome undesired effects like feature broadening seen in single projection images.

Effect of Oxygen inhibition

Oxygen inhibition has long plagued free-radical polymerization processes. Molecular oxygen scavenges the free radicles and either prolong the photocuring process or altogether inhibits it depending on the amount of dissolved oxygen and the provided energy. It is known to react with active radicals and generate dead chain ends, thus preventing reaction propagation [19, 20]. This issue is more pronounced in low-intensity curing processes that use UVA cure, such as the one used in this research. As discussed in the previous section, the temporal effect is believed to arise primarily due to oxygen inhibition. During the first exposure, a part of the energy is used to scavenge the oxygen free radicals present in the resin. If the time delay is small enough to replenish the consumed oxygen, all of the input energy is used for photopolymerization resulting in thicker features. This is dependent on resin viscosity, available oxygen, irradiation, and thermal effects. **Figure *5*** (a) shows the decay function of oxygen inhibitory effects. It is necessary to either account for the dissolved oxygen while modeling the process or finds ways to eliminate the oxygen. Despite the relative maturity of DLP printing, this effect has not yet been quantified.

There are numerous physical and chemical ways to reduce oxygen inhibition. Using higher viscosity polymers or increasing the exposure time by slower cure speeds can help mitigate this effect [21, 22]. Prolonged curing at lower irradiance is not always viable as it can lead to longer printing times, which is not desirable. Other potential ways of mitigating oxygen inhibition are increasing the free radical concentration by increasing the photoinitiator concentration or by increasing the UV intensity. While increasing the photoinitiator concentration is possible, it is not always practical, especially in commercial resins. UV intensity augmentation magnifies the sphere of influence by light bleeding, thus giving rise to spatial proximity effects. Removing oxygen from the cure zone by displacing it with inert gas can help mitigate the effect without chemically transforming the resin or increasing energy requirements. **Figure *6*** (b) shows that when the amount of dissolved oxygen is higher, the printed features are about 15% smaller than the control. This can be attributed to the fact that more energy is consumed to quench the oxygen requiring a longer exposure to overcome the energy barrier, resulting in weaker propagation chains that take longer to polymerize. On the other hand, the features in the oxygen-deprived environment, as seen in **Figure *6*** (c), are approximately 32% larger as more energy is available for actual polymerization.

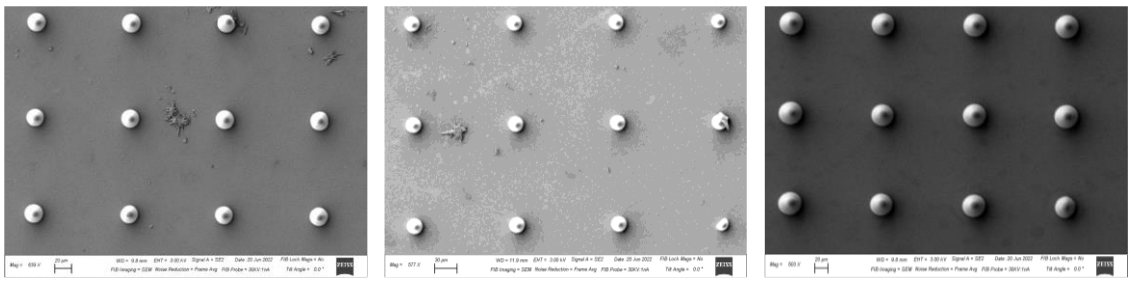

(a) (b) (c)

Figure 6 Effect of oxygen as seen in the spatial domain for (a) stock/control resin, (b) resin with an oxygen-rich environment, and (c) resin with an oxygen-deprived environment. (SEM scale bar = 20 μm for (a), (c) and 30 μm for (b))

As discussed in the previous section, the temporal effect stems from the oxygen inhibitory properties. When the time delay is more, it allows for more time to replenish the oxygen used during the first exposure, thus returning the resin to the status quo and giving rise to uniform features. On the other hand, when the time delay is short, the oxygen consumed during the first exposure is not restored, thus utilizing most of the energy from the second exposure for polymerization, giving rise to thicker features, as seen in **Figure *7*** (b). When the resin is deprived of oxygen, the effect is much more subtle, even when the time delay is small. **Figure *7*** (c) shows the results after repeating the sequential exposure experiment with a 10s delay in an oxygen-deprived resin. The minute non-uniformity in the parts from the two exposures might be because of the process limitations to eliminate all of the oxygen. Though the spatial effect discussed in the previous sections primarily arises due to the light bleeding into neighboring pixels, we believe oxygen too plays a role. When the features are closely packed, the effective energy per unit area is more, causing the oxygen to get quenched faster, thus leaving more energy available for actual polymerization. On the other hand, when the gap between the features is more prominent, it takes longer for the oxygen to get consumed as the energy density is lower, thus giving smaller than desired features for the same exposure. This can also explain why polymerization is difficult when the feature size gets smaller.

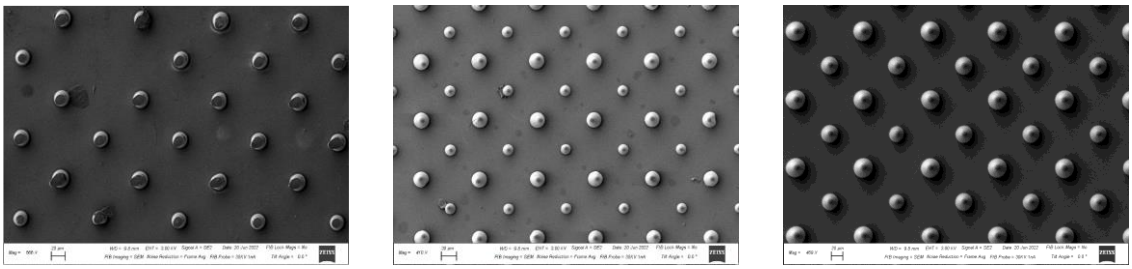

(a) (b) (c)

Figure 7 Temporal effect of proximity (a) with control/stock resin time delay 60s, (b) with control/stock resin time delay 10s, and (c) with oxygen-deprived resin time delay 10s (SEM scale bar = 20 μm)

Validation and robustness

The proximity effect is more pronounced at micron scale, but it exists at larger scale as well. Experiments were conducted to observe this effect at macro scale to validate our claims and

demonstrate the robustness of our designed system. DLP setup used in this research allowed us to change the magnification of the system to 1.5:1. PEGDA 250 UV resin was used for this experiment. The designed schlieren setup allowed us to observe the polymerization process from the side and revealed how the proximity effect takes place. Voxel growth dynamics were studied for macro scaled parts using the designed schlieren system.

Figure 8 shows the voxel growth at different time stamps during vat polymerization for a 100 µm feature. ***Figure 8*** (a), (b), and (c) represent the voxel growth during the first projection. They show the nonlinear photopolymerization process that is terminated at 5 seconds. To study the temporal effect, second mask was projected with alternating patterns after a time delay of 10 seconds. ***Figure 8*** (d), (e), and (f) represent the voxel growth during second exposure. As evident from the images the growth rate during second exposure is much faster as most of the energy is utilized for polymerization rather than oxygen quenching. For the same exposure, the voxels from second projection are relatively larger. Schlieren system allowed us to characterize this process in-situ thus eliminating the discrepancies that might occur during cleaning post processing.

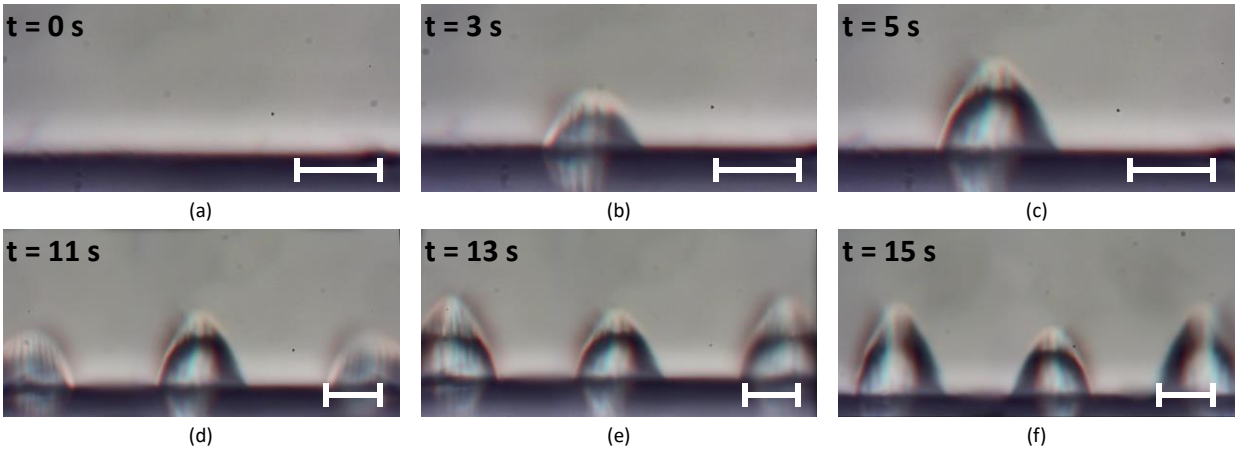

Figure 8 Temporal proximity effect observed from the side at different time stamps (Scale bar = 100 µm)

Conclusion and Future work

In this paper, we investigated the proximity effects in spatial and temporal scales during DLP printing using experimental data. Different patterned structures were exploited to study the influence of structural features in DLP on a time and micrometer spatial scale. The measurements indicate that light spreading in the sphere of influence strongly affects the material response. The spatial response extends beyond the actual projections when the feature density is high, as each feature is influenced by its immediate neighbors. The temporal effect arises when multiple projections are used subsequently and were seen to have an effect within a specific period. We also studied the role of oxygen in free radical polymerization. It was observed that the amount of oxygen greatly influences the feature dimensions, and the temporal effect is primarily due to oxygen inhibition. The research also, for the first time, demonstrates techniques for observing the voxel growth and the interactions between adjacent features in-situ. The temporal proximity as

observed from the schlieren system has opened up new possibilities for developing data driven models specific to patterned periodic structures that consider the inter-feature interactions.

Although oxygen inhibition also affects the spatial proximity effects, further experiments need to be conducted to pinpoint the significant contributor, radical and/or oxygen, to this proximity effect. This research doesn't consider thermal effects that might play a role in determining the spatio-temporal proximity characteristics. While the effects were observed and characterized in this research, more data needs to be collected to derive better empirical models from showcasing how the photopolymerization process takes place in single-shot DLP printing. This research has paved the way toward developing optimization models for printing densely packed high-resolution micron scaled features with enhanced uniformity and tunability. These will be studied in future work.

Acknowledgments

The authors would like to gratefully acknowledge the support from the U.S. National Science Foundation (NSF) through the award ECCS -2111056.

References

1. Yuan, C., et al., *Ultrafast three-dimensional printing of optically smooth microlens arrays by oscillation-assisted digital light processing.* ACS applied materials & interfaces, 2019. **11**(43): p. 40662-40668.
2. Li, Y., et al., *Bioinspired functional surfaces enabled by multiscale stereolithography.* Advanced Materials Technologies, 2019. **4**(5): p. 1800638.
3. Yan, C., et al., *3D printing of bioinspired textured surfaces with superamphiphobicity.* Nanoscale, 2020. **12**(5): p. 2924-2938.
4. Dabbagh, S.R., et al., *3D-printed microneedles in biomedical applications.* Iscience, 2021. **24**(1): p. 102012.
5. Cordeiro, A.S., et al., *Two-photon polymerisation 3D printing of microneedle array templates with versatile designs: application in the development of polymeric drug delivery systems.* Pharmaceutical research, 2020. **37**(9): p. 1-15.
6. Hohmann, J.K., et al., *Three-Dimensional μ-Printing: An Enabling Technology.* Advanced Optical Materials, 2015. **3**(11): p. 1488-1507.
7. Sun, H.-B. and S. Kawata, *Two-photon photopolymerization and 3D lithographic microfabrication.* NMR• 3D Analysis• Photopolymerization, 2004: p. 169-273.
8. Weisgrab, G., et al., *3D Printing of large-scale and highly porous biodegradable tissue engineering scaffolds from poly (trimethylene-carbonate) using two-photon-polymerization.* Biofabrication, 2020. **12**(4): p. 045036.
9. Huang, Z., et al., *Two-photon polymerization nanolithography technology for fabrication of stimulus-responsive micro/nano-structures for biomedical applications.* Nanotechnology Reviews, 2020. **9**(1): p. 1118-1136.
10. Choi, J.-W., Y. Lu, and R.B. Wicker, *4 Projection Microstereolithography as a Micro-Additive Manufacturing Technology.* Additive Manufacturing: Innovations, Advances, and Applications, 2015: p. 101.

11. Arnoux, C., et al., *Understanding and overcoming proximity effects in multi-spot two-photon direct laser writing.* Additive Manufacturing, 2022. **49**: p. 102491.
12. Tan, D., et al., *Reduction in feature size of two-photon polymerization using SCR500.* Applied physics letters, 2007. **90**(7): p. 071106.
13. Waller, E.H. and G. Von Freymann, *Spatio-temporal proximity characteristics in 3D μ-printing via multi-photon absorption.* Polymers, 2016. **8**(8): p. 297.
14. Zhou, C., Y. Chen, and R.A. Waltz. *Optimized mask image projection for solid freeform fabrication*. in *International Design Engineering Technical Conferences and Computers and Information in Engineering Conference*. 2009.
15. Settles, G.S., *Schlieren and shadowgraph techniques: visualizing phenomena in transparent media*. 2001: Springer Science & Business Media.
16. Huang, C., J.W. Gregory, and J.P. Sullivan, *A modified schlieren technique for micro flow visualization.* Measurement Science and Technology, 2007. **18**(5): p. N32.
17. Agarwal, S., et al. *On refractive optical flow*. in *European Conference on Computer Vision*. 2004. Springer.
18. Mazumdar, A., *Principles and techniques of schlieren imaging systems.* 2013.
19. Mandal, J., K. Zhang, and N.D. Spencer, *Oxygen inhibition of free-radical polymerization is the dominant mechanism behind the "mold effect" on hydrogels.* Soft Matter, 2021. **17**(26): p. 6394-6403.
20. Ligon, S.C., et al., *Strategies to reduce oxygen inhibition in photoinduced polymerization.* Chemical reviews, 2014. **114**(1): p. 557-589.
21. Schwalm, R., *UV coatings: basics, recent developments and new applications.* 2006.
22. Jo Ann Arceneaux, C.B., Kevin Poelmans *Use of Amino Acrylates to Reduce Photoinitiator Concentration or Increase Cure Speed in UV LED-Curable OPVs and Flexo Inks*. 2018, Paint & Coating Industry: PCI Mag.